SUPPLEMENTARY INFORMATION

Dibenzocyclooctyne Conjugation Enhances Antigen Cross-Presentation and T cell Killing for Potent Cancer Vaccines

Zhiguo Li[a,b,§], Tengyao Wang[a,c,§], Weifan Li[a,c,§], Peiyu Yu[d], Kangxiu Wu[e], Chanjuan Su[a], Fuxiang Wang[a], Huosheng Zhou[a], Fan Lan[a], Yaofeng Zhou[f,g], Kaimin Cai[h], Menghua Xiong[i,j], Songyin Huang[c,k], Jianjun Cheng[f,g,l,*], Minmin Xiong[c,*], Kaiting Yang[i,j,*], and Yan Bao[a,m,*]

[a]*Guangdong Provincial Key Laboratory of Malignant Tumor Epigenetics and Gene Regulation, Sun Yat-Sen Memorial Hospital, Sun Yat-Sen University, Guangzhou 510120, China*

[b]*Breast Tumor Center, Sun Yat-sen Memorial Hospital, Sun Yat-sen University, Guangzhou 510120, China*

[c]*Biotherapy Center, Sun Yat-Sen Memorial Hospital, Sun Yat-Sen University, Guangzhou 510120, China*

[d]*Department of Chemistry, School of Science, Westlake University, Hangzhou 310030, China*

[e]*Department of Clinical Laboratory, Sun Yat-sen Memorial Hospital, Sun Yat-sen University, Guangzhou 510120, China*

[f]*School of Engineering, Westlake University, Hangzhou 310030, China*

[g]*Institute of Advanced Technology, Westlake Institute for Advanced Study, Hangzhou 310024, China*

[h]*Surio Therapeutics Co., Ltd, Hangzhou 310012, China*

[i]*School of Biomedical Sciences and Engineering, South China University of Technology, Guangzhou International Campus, Guangzhou 511442, China*

[j]*National Engineering Research Centre for Tissue Restoration and Reconstruction, South China University of Technology, Guangzhou 510006, China*

[k]*Guangdong Provincial Key Laboratory of Cancer Pathogenesis and Precision Diagnosis and Treatment, Shenshan Medical Center, Sun Yat-sen Memorial Hospital, Sun Yat-sen University, Shanwei 516621, China*

[l]*School of Engineering and Research Center for Industries of the Future, Westlake University, Hangzhou 310030, China*

[m]*Nanhai Translational Innovation Center of Precision Immunology, Sun Yat-Sen Memorial Hospital, Foshan 528200, China*

[*]E-mail: baoy5@mail.sysu.edu.cn; yangkt@scut.edu.cn; xiongmm5@mail.sysu.edu.cn; chengjianjun@westlake.edu.cn

§ Z.Li, T.Wang and W.Li contributed equally to this work

Table of Contents

Additional Materials and Methods

Cells and animals

B16-F10, B16-OVA and DC2.4 cells were maintained in RPMI-1640 medium supplemented with 10% fetal bovine serum (FBS), 1% penicillin-streptomycin (P/S) and cultured at 37 °C in a humidified incubator with 5% CO_2. Female C57BL/6 mice (5-week-old) were obtained from Zhuhai BesTest Bio-Tech Co., Ltd (China) and housed in the Nanhai Laboratory Animal Center of Sun Yat-sen Memorial Hospital. All animals were maintained under specific pathogen-free (SPF) conditions, with a 12-hour light/dark cycle at 25 °C, and provided ad libitum access to food and water.

Preparation and characterization of THDBCO-PEG$_4$-NHS

DBCO-PEG$_4$-COOH (>98%, CAS: 1537170-85-6) was purchased from Shanghai Haohong Scientific Co., Ltd. Nuclear magnetic resonance (NMR) spectra were recorded on a Bruker AVANCE 400 MHz spectrometer. Chemical shifts (δ) are reported in ppm relative to residual solvent signals ($CDCl_3$: δ 7.26 for ^{1}H NMR). Liquid Chromatography-Mass Spectrometry (LC-MS) were recorded on Shimadzu LCMS-8060 system. The synthetic procedure is illustrated in Scheme S1.

Synthesis of 3-{[13,16-dioxo-16-(5,6,11,12-tetrahydrodibenzo[1,2-f:1',2'-b]azocin-5-yl)-12-aza-3,6,9-trioxahexadec-1-yl]oxy}propanoic acid (2): To a solution of DBCO-PEG$_4$-COOH (1.0 g, 1.80 mmol) in methanol (MeOH, 20 mL) was added platinum(IV) oxide (PtO_2, 409 mg, 1.80 mmol). The mixture was stirred under a hydrogen atmosphere (balloon pressure) at room temperature for 2 h. Progress of the reaction was monitored by LC-MS. Upon completion, the reaction mixture was filtered to remove the catalyst, and the filtrate was concentrated in vacuo to afford compound 2 as a yellow oil (801 mg, 79% yield). The crude product was used directly in the next step without further purification. (ESI-MS: $[M+H]^+$: 557.5)

Synthesis of N-{15-[(2,5-dioxopyrrolidin-1-yl)oxy]-15-oxo-3,6,9,12-tetraoxapentadec-1-yl}-4-oxo-4-(5,6,11,12-tetrahydrodibenzo[1,2-f:1',2'-b]azocin-5-yl)butanamide (3): To a solution of compound 2 (500 mg, 0.90 mmol) in dichloromethane (DCM, 20 mL) were sequentially added O-(benzotriazole-1-yl)-N,N,N',N'-tetramethyluronium tetrafluoroborate (TSTU, 352 mg, 1.17 mmol) and N,N-diisopropylethylamine (DIEA, 233 mg, 1.80 mmol) at room temperature. The mixture was stirred at room temperature for 2 hours. The progress was monitored by LC-MS. The mixture was concentrated in vacuo, and the residue was purified by column chromatography (SiO_2, eluent: DCM/MeOH gradient from 0% to 20% MeOH) to afford compound 3 as a colorless oil (95 mg, 16% yield). ESI-MS: $[M+H]^+$: 654.5. ^{1}H NMR (400 MHz, $CDCl_3$): δ 7.17-6.99 (m, 8H), 6.83 (s, 1H), 5.73 (d, J = 14.4 Hz, 1H), 4.11 (d, J = 14.4 Hz, 1H), 3.85 (t, J = 6.4 Hz, 2H), 3.77-3.59 (m, 12H), 3.55 (t, J = 5.2 Hz, 2H), 3.48-3.37 (m, 2H), 3.29-3.12 (m, 2H), 2.89 (t, J = 6.4 Hz, 2H), 2.88-2.79 (m, 6H), 2.62-2.49 (m, 2H), 2.47-2.36 (m, 1H), 2.26-2.13 (m, 1H). The ^{1}H NMR spectra of THDBCO-PEG$_4$-NHS is illustrated in Figure S1.

Preparation and characterization of DBCO-OVA and structural analogs

OVA was dissolved in 0.1 M Na_2CO_3/$NaHCO_3$ buffer (pH = 9.0) and mixed with DBCO-PEG$_4$-NHS at a molar ratio of 1:10. The reaction mixture, containing 10% DMSO, was stirred at 4 °C in the dark for 8 hours. The reaction was terminated by the addition of 5 M NH_4Cl to a final concentration of 50 mM.

Free DBCO was removed using a 30 kDa-filter ultrafiltration tube, and the resulting concentrated DBCO-OVA was collected. Final protein concentration was determined by the BCA assay. DBCO modification was verified via a click reaction with an azide-functionalized Cy5 probe (N_3-Cy5). DBCO-OVA was incubated with 50 μM N_3-Cy5 for 1 hour, washed with TBST buffer, and analyzed by SDS-PAGE followed by polyvinylidene fluoride (PVDF) membrane transfer. Cy5 fluorescence overlapping the OVA band was visualized using a fluorescence scanner. Zeta potential was measured using a Zetasizer Nano system. The degree of DBCO conjugation was characterized by MALDI-TOF mass spectrometry.

BCN-OVA, m-PEG_4-OVA, and THDBCO-OVA were synthesized in a similar procedure with BCN-PEG_4-NHS, m-PEG_4-NHS, and THDBCO-PEG_4-NHS as the starting materials. BCN-PEG_4-NHS were purchased from MACKLIN and m-PEG_4-NHS were purchased from MedChemExpress.

Preparation of DBCO-modified tumor cell lysate (DBCO-TCL)

Tumor cells were cultured to confluence, washed with PBS, digested with 0.25% trypsin, and collected after centrifugation at 1200 rpm for 5 min. Repeated freeze-thaw cycles were performed three times to generate tumor cell lysates (TCL). The lysates were centrifuged at 1500 rpm for 15 min and the supernatant was further filtered a 0.22 μm membrane. Total protein concentration in the supernatant was determined using the BCA assay. The filtered TCL was aliquoted and stored at -80 °C until use. For DBCO conjugation, TCL was dissolved in 0.1 M Na_2CO_3/$NaHCO_3$ buffer (pH = 9.0) to yield a 2 mg/mL solution. DBCO-PEG_4-NHS was added at a mass ratio of 6:1 (TCL: DBCO-PEG_4-NHS), and 10% DMSO was included in the reaction mixture. The reaction was stirred at 4 °C in the dark for at least 8 hours. The conjugation was terminated by the addition of 5 M NH_4Cl to a final concentration of 50 mM. The resulted DBCO-TCL was stored at 4 °C for subsequent use.

Evaluation of antigen uptake by DC2.4 cells using confocal microscopy

DC2.4 cells were detached using 0.25% trypsin, resuspended and seeded into 24-well plate (CCP06-024, BIOLAND), then incubated overnight at 37 °C in a 5% CO_2 incubator. Cells were subsequently incubated with 50 μg/mL OVA-FITC or DBCO-OVA-FITC, respectively. After 4 hours and 12 hours of incubation, cells were washed three times with PBS and then incubated with 100 μL of DMEM containing 1× Hoechst dye for 10 minutes in the dark. Fluorescence images were acquired using a confocal laser scanning microscope (Olympus FV3000), collecting signals from FITC and Hoechst channels.

Preparation of BMDCs

Bilateral femurs and tibias were harvested from C57BL/6 mice, the surrounding muscle tissue was carefully removed and the bones were briefly disinfected in 70% ethanol before being transferred into sterile PBS. Bone marrow cavities were flushed with PBS to collect bone marrow cells. After treatment with red blood cell lysis buffer, the cells were centrifuged again and resuspended in complete RPMI-1640 medium supplemented with 10% heat-inactivated fetal bovine serum (FBS) and 1% P/S. Recombinant murine GM-CSF (20 ng/mL) and IL-4 (10 ng/mL) were added, and the cells were

incubated at 37 °C in a humidified atmosphere containing 5% CO_2. On days 2 and 4, one-quarter of the culture medium was replaced with fresh medium containing cytokines. On day 7, non-adherent and loosely adherent cells were collected for subsequent experiments.

Detection of antigen uptake, presentation, and maturation of BMDCs by flow cytometry

BMDCs were seeded in 24-well plates and incubated overnight at 37 °C in a 5% CO_2 incubator. The following day, cells were subsequently incubated with 50 μg/mL OVA or DBCO-OVA or equivalent volume of PBS for 12 to 48 hours. After incubation, cells were collected and subjected to antibody staining. For antigen uptake analysis, cells were stained with PE-conjugated anti-mouse CD11c antibody (BioLegend, N418). For antigen presentation assays, cells were stained with PE-conjugated anti-CD11c (BioLegend, N418) and PE-Cy7-conjugated anti-H-2K^b/SIINFEKL (BioLegend, 25-D1.16) antibodies. For maturation analysis, BMDCs were stained with a panel of antibodies: CD11c (PE) (BioLegend, N418), MHC-II (AF700) (BioLegend, M5/114.15.2), CD80 (FITC) (BioLegend, 16-10A1), CD86 (BV650) (BioLegend, GL-1), and CD40 (PerCP/Cy5.5) (BioLegend, 3/23). All staining procedures were performed on ice in the dark for 30 minutes, followed by washing with PBS twice. DAPI (5 μg/mL) was added immediately before flow cytometry to distinguish dead cells. All samples were analyzed using a CytoFLEX S flow cytometer (Beckman CytoFLEX, USA), and data were processed using FlowJo v10 software.

ELISA detection of cytokine secretion by BMDCs

BMDCs were seeded in a 24-well plate and incubated overnight at 37 °C in a 5% CO_2 incubator. The following day, cells were incubated with 50 μg/mL OVA, DBCO-OVA or equivalent volume of PBS for 48 hours. After incubation, culture supernatants were collected, and the concentrations of IL-1β and IL-6 were quantified using commercial ELISA kits (CSB-E08054m and CSB-E04639m, CUSABIO, https://www.cusabio.com/), while IL-12p70 and TNF-α levels were measured with ELISA kits (SEKM-0013 and SEKM-0034, Solarbio, Shanghai, China), all according to the manufacturers' instructions.

Isolation and cytotoxicity detection of OT-1 T cells

Spleens were harvested from OT-1 mice and processed into single-cell suspensions. $CD8^+$ T cells were isolated using a commercial magnetic bead separation kit (BioLegend) according to the manufacturer's instructions. BMDCs were seeded in a 24-well plate at a density of 5×10^5 cells per well and stimulated with 50 μg/mL OVA or DBCO-OVA or equivalent volume of PBS for 24 hours. B16-OVA tumor cells were digested, resuspended in RPMI-1640 supplemented with 5 μM CFSE, at 37 °C for 10 minutes. After washing with PBS, CFSE-labeled cells were ready for co-culture. Purified $CD8^+$ T cells, antigen-pulsed BMDCs, and CFSE-labeled B16-OVA cells were mixed at a ratio of 10:5:1, and co-cultured in a 24-well plate (5×10^4 tumor cells per well) for 24 hours at 37 °C in a CO_2 incubator. After incubation, cells were harvested using trypsin digestion, stained with DAPI, and analyzed by flow cytometry. The number of $CFSE^+DAPI^-$ live tumor cells was quantified using counting beads. Survival rate of tumor cell was calculated as follows: survival rate (%) = (live tumor cells / bead count in experimental well) ÷ (live tumor cells / bead count in control well) × 100%. This value was used to

evaluate the antigen-specific cytotoxic activity of $CD8^+$ T cells.

NF-κB pathway activation analysis via western blot

BMDCs were harvested after antigen stimulation, and total protein was extracted using lysis buffer (Beyotime, China). Protein concentration was determined using the BCA assay. Samples were denatured and separated by SDS-PAGE, followed by transfer onto PVDF membranes. After blocking in 5% skim milk, membranes were sequentially incubated with primary antibodies against p-p65(Cell Signaling, 93H1), p65 (Santa Cruz, sc8008), p-IκBα (Selleck, B13N13), IκBα (Santa Cruz, sc-1643), and GAPDH (Santa Cruz, sc-365062), and HRP-conjugated secondary antibodies. Chemiluminescent substrate (EpiZyme) was applied to visualize protein bands, and signals were captured using an imaging system (Bio-Rad).

p65 nuclear translocation analysis by western blot

BMDCs were harvested after antigen stimulation, and nuclear proteins were extracted according to the manufacturer's instructions of a commercial cell nuclear extraction kit (Beyotime, China). Nuclear protein samples were subjected to western blot analysis following the same procedure described above, using primary antibodies against p65 (Santa Cruz, sc-8008), HDAC1 (Proteintech, 10197-1-AP), and GAPDH (Santa Cruz, sc-365062) to assess p65 nuclear translocation.

Immunofluorescence staining

DC2.4 cells were seeded in a 24-well plate containing sterile glass coverslips and incubated with the appropriate treatments before fixation. Permeabilization was performed using 100 μL of Triton X-100. Following blocking, samples were incubated sequentially with primary antibody against p65 (Santa Cruz, sc8008) and a Cy3-conjugated secondary antibody (KERONG), with thorough PBS washes between steps. After staining, cells were mounted using an anti-fade mounting medium containing DAPI and covered with a coverslip. Fluorescence images were acquired using a confocal laser scanning microscope (Olympus FV3000) for further analysis.

Detection of antigen uptake and maturation of pulmonary APCs

Mice were intravenously injected with OVA-FITC or DBCO-OVA-FITC (for uptake analysis), or with OVA or DBCO-OVA (for maturation analysis). After 24 hours, lungs were harvested to prepare single-cell suspensions for staining. For uptake analysis, cells were stained with Fixable Viability Stain 510 (BD), PerCP-Cy5.5 anti-mouse CD45 (BioLegend, 30-F11), APC/Fire™ 750 anti-mouse F4/80 (BioLegend, BM8), BV785 anti-mouse CD11b (BioLegend, M1/70), and BV421 anti-mouse CD11c (BioLegend, N418). For maturation analysis, cells were stained with Fixable Viability Stain 510 (BD), FITC anti-mouse CD45 (BioLegend, S18009F), APC/Fire™ 750 anti-mouse F4/80 (BioLegend, BM8), BV421 anti-mouse CD11c (BioLegend, N418), APC anti-mouse CD80 (BioLegend, 16-10A1), and BV605 anti-mouse CD86 (BioLegend, PO3). All staining procedures were performed on ice. After staining, cells were washed with PBS and passed through a cell strainer before analysis. Samples were analyzed using a CytoFLEX S flow cytometer (Beckman Cytoflex LX).

Quantification of OVA-specific $CD8^+$ T cell responses Using *in vivo*

Mice were i.v. injected with 100 μg OVA or DBCO-OVA, or equivalent volume of PBS as control. On day 7 post-immunization, spleens were harvested from unimmunized donor mice to prepare single-cell suspensions,

followed by red blood cell lysis. Splenocytes were divided into two groups: pulsed with $OVA_{257-263}$ peptide, or untreated, and labeled with different concentrations of CFSE to distinguish them, $CFSE^{high}$ (peptide-pulsed) and $CFSE^{low}$ (unpulsed). After staining, equal numbers of $CFSE^{high}$ and $CFSE^{low}$ cells were mixed and co-injected intravenously into the immunized recipient mice. Sixteen hours later, lungs and spleens were collected to prepare single-cell suspensions. DAPI staining was performed to exclude dead cells. Samples were analyzed by flow cytometry, and the ratio of $CFSE^{high}$ to $CFSE^{low}$ cells was quantified to evaluate OVA-specific CTL activity *in vivo*.

Tumor model establishment

5-week-old female C57BL/6 mice were used to establish both subcutaneous solid tumor and lung metastasis models. For the subcutaneous tumor model, mice were shaved on the dorsal side and injected subcutaneously with 5×10^5 B16-F10 or B16-OVA cells in PBS suspension. Once tumors became palpable, tumor length and width were measured using a caliper, and tumor volume was calculated using the formula: volume = length × $width^2$ × 0.5. When tumors reached approximately 50 mm^3, mice were randomly assigned to experimental groups and treated accordingly. For the lung metastasis model, 2×10^5 B16-OVA cells were injected via tail vein to induce pulmonary metastases. Starting on day 4 post-injection, mice were assigned to treatment groups, and body weight was monitored every 3-4 days to assess disease progression.

Flow cytometry analysis

Tumor tissues, spleens, or lungs were harvested and processed into single-cell suspensions for flow cytometric analysis. Immune cells were isolated from tumor tissues following enzymatic digestion and Percoll density gradient centrifugation, followed by red blood cell lysis. For DC maturation analysis, cells were stained with Fixable Viability Stain 510 (BD), APC/Cy7 anti-mouse CD45 (BioLegend, I3/2.3), PE anti-mouse CD11c (BioLegend, N418), FITC anti-mouse CD80 (BioLegend, 16-10A1), BV650 anti-mouse CD86 (BioLegend, GL-1), and AF700 anti-mouse MHC-II (BioLegend, M5/114.15.2). For T cell quantification, cells were stained with Fixable Viability Stain 510 (BD), APC/Cy7 anti-mouse CD45 (BioLegend, I3/2.3), BV605 anti-mouse CD3 (BioLegend, 17A2), PerCP-Cyanine5.5 anti-mouse CD4 (BioLegend, RM4-5), and AF700 anti-mouse CD8 (BioLegend, 53-5.8). To assess T cell effector molecule expression, cells were stained with Fixable Viability Stain 510 (BD), APC/Cy7 anti-mouse CD45 (BioLegend, I3/2.3), BV605 anti-mouse CD3 (BioLegend, 17A2), PerCP-Cyanine5.5 anti-mouse CD4 (BioLegend, RM4-5), AF700 anti-mouse CD8 (BioLegend, 53-5.8), APC anti-mouse Granzyme B (BioLegend, QA16A02), and PE-Cy7 anti-mouse IFN-γ (BioLegend, XMG1.2). Gating strategies of T cells from tumor tissues or spleens were shown in **figure S11-S13**.

Molecular docking process

The crystal structure of MHC class I ligand SIINFEKL-PEG_4-DBCO (chicken ovalbumin epitope OVA antigenic peptide modified with DBCO-PEG_4 at the ε-N of lysine residue) was generated using ChemDraw and converted into a 3D structure with Chem3D. The structure was energy-minimized using the MM2 force field until convergence. The crystal structure of

SIINFEKL-bound mouse MHC class I molecule[1] (H2-K^b, PDB code: 3P9L) was obtained from the Protein Data Bank (PDB; http://www.rcsb.org/pdb/) as the 3D structure of a H2-K^b in complex with OVA antigenic peptide SIINFEKL.

Docking studies between SIINFEKL-PEG_4-DBCO and H2-K^b ligand binding domain were carried out by using AutoDock Vina 1.2.5.[2,3] A grid box of 22.5 × 47.25 × 47.25 $Å^3$ was centered on the original ligand coordinates, with a grid spacing of 0.375 Å. The exhaustiveness was set to 8, up to 9 binding modes were generated, and other parameters were set to default values.

After docking, nine binding modes as the top-ranked poses were present for each docked ligand, and the binding mode showed the similar orientation in accordance with that of SIINFEKL in crystal complex owns the highest absolute value of affinity (affinity = -7.8 kcal/mol) was chose as the final binding mode, visualized using PyMOL. Figure S5 showed binding modes predicted from molecular docking study for SIINFEKL-PEG_4-DBCO toward H2-K^b (3P9L) ligand binding domain.

Data visualization and statistical analysis

Statistical analyses were performed using GraphPad Prism v9.4.0. All figures were generated using GraphPad Prism v9.4.0. Kaplan–Meier survival curves were analyzed using the log-rank test. One-way ANOVA was used for comparisons involving more than two groups, while two-way ANOVA was used to analyze the effects of two independent factors. Results are presented as mean ± standard deviation (mean ± SD). A P-value < 0.05 was considered statistically significant. In all cases, significance levels are defined as: ns, $P \geq 0.05$, *$P < 0.05$, **$P < 0.01$, ***$P < 0.001$, ****$P < 0.0001$.

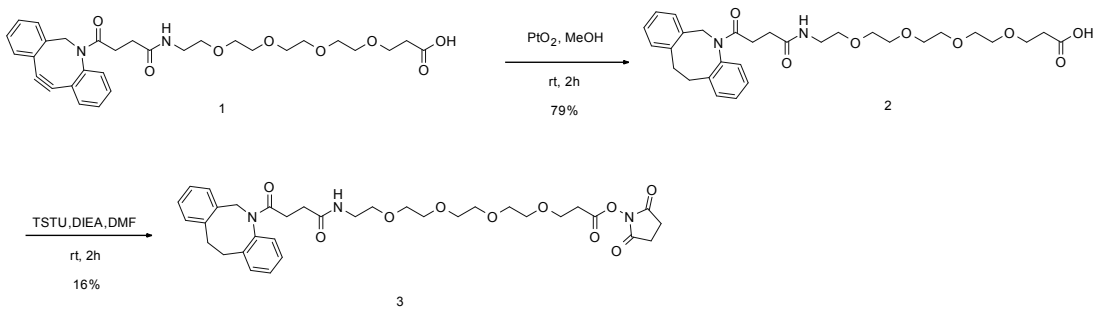

Scheme S1. Schematic illustration of the synthetic route of THDBCO-PEG$_4$-NHS.

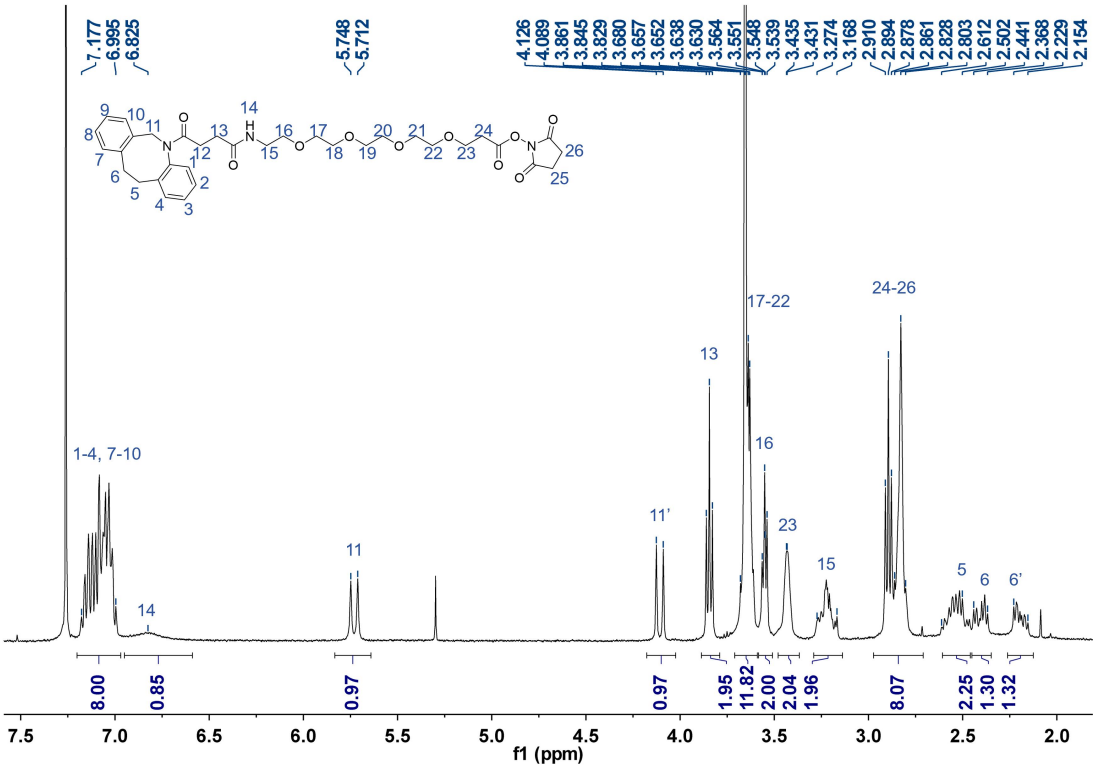

315

316 **Figure S1.** ^{1}H NMR spectrum of THDBCO-PEG$_4$-NHS.

317

318

319

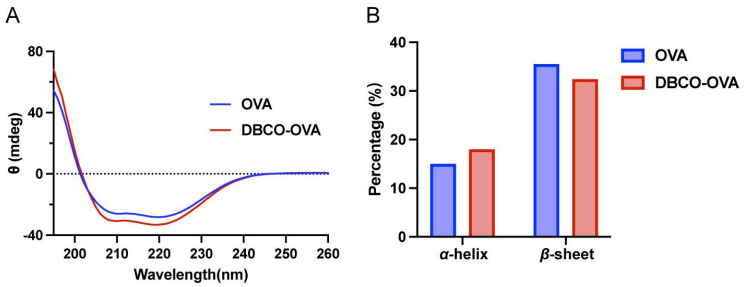

320

321 **Figure S2.** CD spectroscopy (A) and quantitative analysis (B) showed that DBCO
322 modification does not exhibit a significant effect on the secondary structure of the OVA
323 protein.

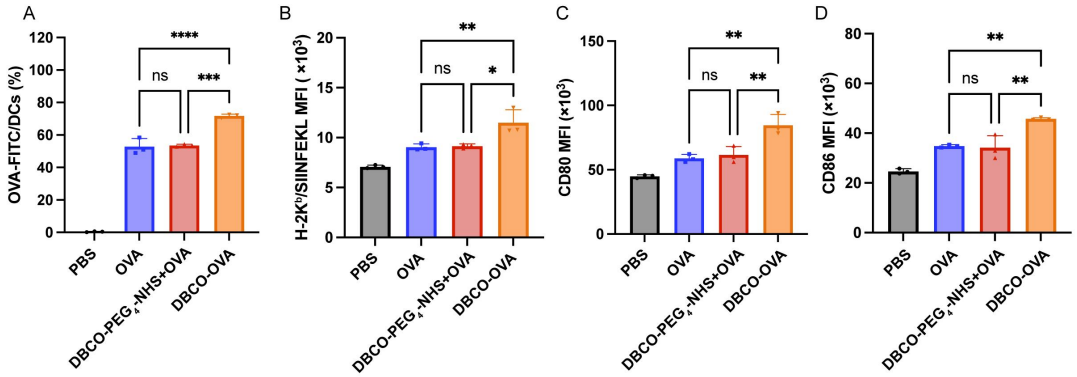

Figure S3. Addition of OVA and DBCO-PEG$_4$-NHS into the cell culture medium does not enhance antigen presentation by DCs. Antigen uptake, antigen presentation, and DC maturation were detected by flow cytometry. (A) Antigen uptake by BMDCs. BMDCs were co-cultured with 50 μg/mL of FITC-labeled OVA, physical mixture of DBCO-NHS and OVA, or DBCO-OVA, for 12 hours. (B) H-2K^b/SIINFEKL presentation on BMDCs detected by flow cytometry. BMDCs were co-cultured with 50 μg/mL of OVA, physical mixture of DBCO-NHS and OVA, or DBCO-OVA, for 24 hours. (C-D) CD80 and CD86 expression on BMDCs. BMDCs were co-cultured for 48 hours. n = 3. Statistical analysis was performed using one-way analysis of variance (ANOVA), and the data are presented as mean ± standard deviation (SD). ns, no significance; *P < 0.05; **P < 0.01; ***P < 0.001; ****P < 0.0001.

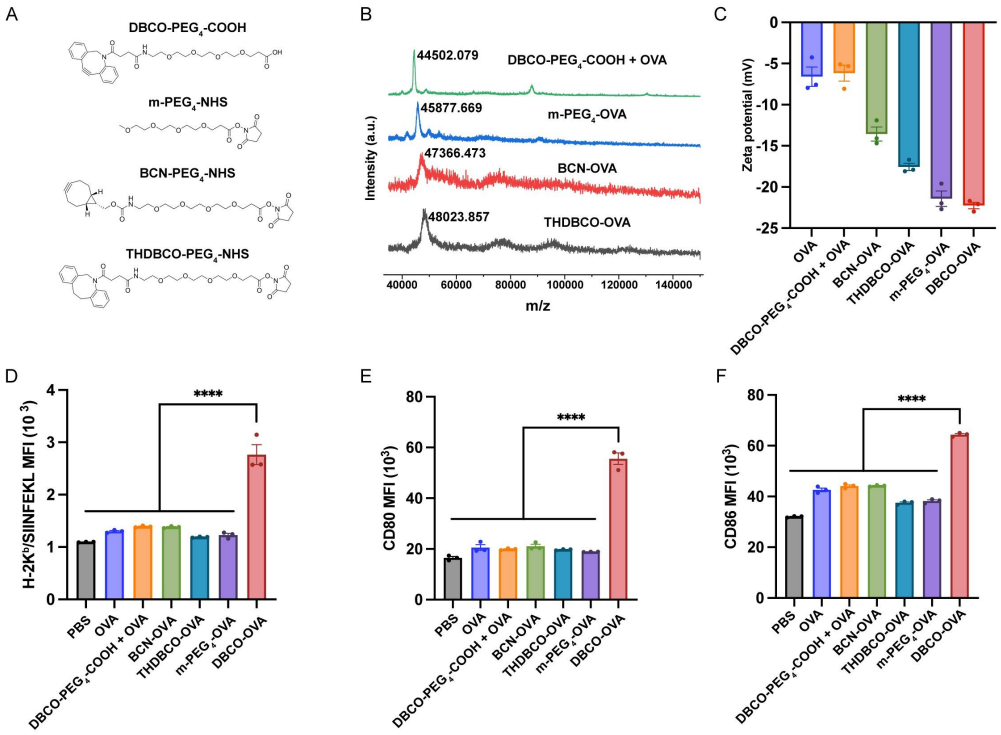

Figure S4. The immunostimulatory effects of DBCO-OVA are dependent on the specific chemical functionality of DBCO. (A) The structure of BCN-PEG$_4$-NHS, THDBCO-PEG$_4$-NHS, m-PEG$_4$-NHS and DBCO-PEG$_4$-COOH. (B) MALDI-TOF mass spectra of DBCO-OVA structural analogs. (C) Zeta potential analysis comparing OVA and DBCO-OVA structural analogs (n = 3). (D) Flow cytometry analysis of H-2K^b-SIINFEKL presentation on the surface of DC2.4 cells following DBCO-OVA and structural analogs treatment. (E and F) Flow cytometry analysis of surface maturation markers (CD80, CD86) on DC2.4 following DBCO-OVA and structural analogs treatment, n = 3. Statistical analysis was performed using one-way ANOVA, and data are presented as mean ± SD. ****P < 0.0001.

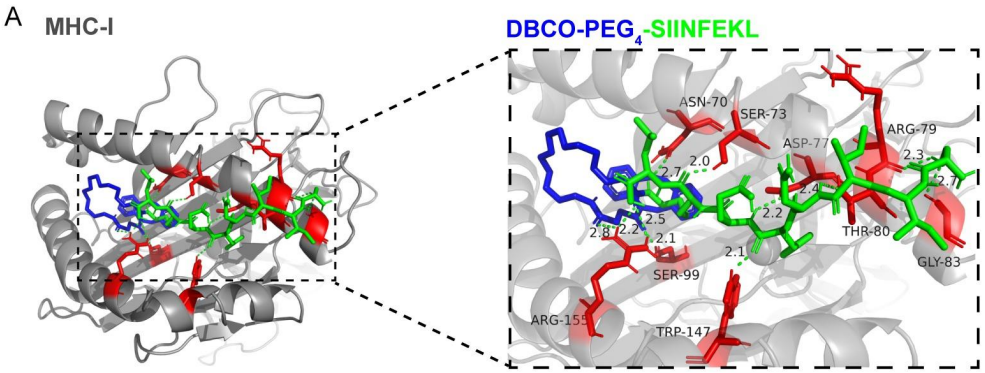

B

Protein-ligand complex	Binding free energy (kcal/mol)
MHC I protein to SIINFEKL	-7.944 ± 0.508
MHC I protein to DBCO-SIINFEKL	-7.444 ± 0.260

Figure S5. DBCO modification did not significantly alter the binding affinity of MHC I to SIINFEKL peptide. (A) The structural conformations of MHC-I and SIINFEKL peptide after the modification of DBCO. (B) The mean binding free energy (with 9 binding modes) of MHC-I to the SIINFEKL peptide, with and without DBCO modification.

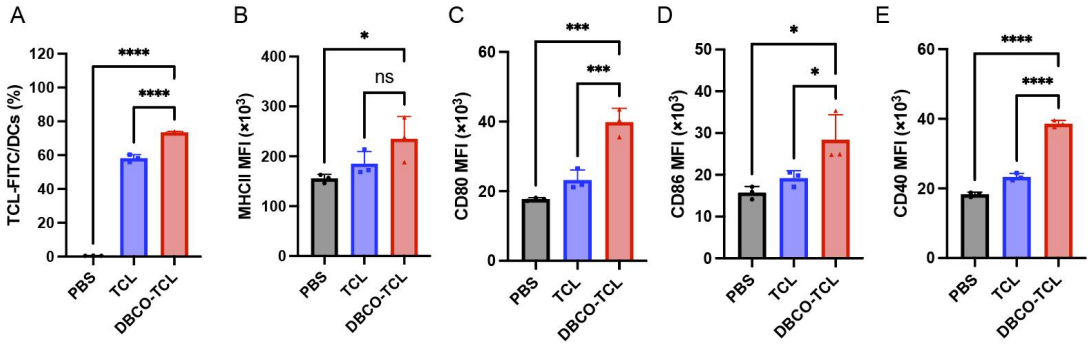

Figure S6. Enhanced DBCO-TCL uptake and maturation in BMDCs. (A) Antigen uptake detected by flow cytometry. BMDCs were co-cultured with 50 μg/mL of TCL or DBCO-TCL for 12 hours, (B-E) Expression of MHC-II, CD80, CD86, and CD40 detected by flow cytometry. BMDCs were co-cultured with 50 μg/mL of TCL or DBCO-TCL for 48 hours. n = 3. Statistical analysis was performed using one-way ANOVA, and data are presented as mean ± SD. ns, no significance; **P* < 0.05; ***P* < 0.01; ****P* < 0.001; *****P* < 0.0001.

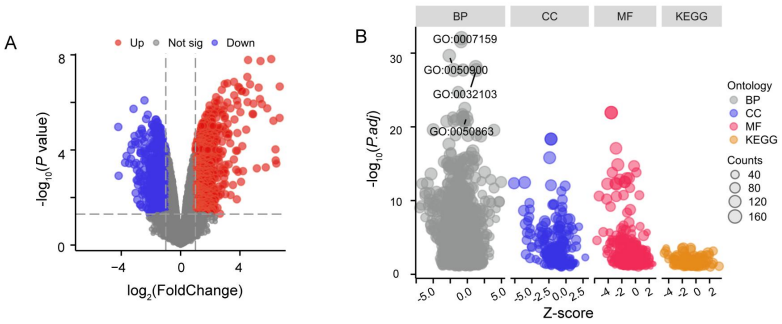

Figure S7. Transcriptomic analysis of BMDCs stimulated with PBS or DBCO-OVA. (A) Volcano plots showing differentially expressed genes in BMDCs stimulated with PBS or DBCO-OVA, where genes with a *P*-value < 0.05 and $|\log_2\text{fold change}| > 0.58$ are considered significantly different. (B) Gene Ontology (GO) and KEGG enrichment analysis of differentially expressed genes, where significant terms and pathways were identified based on a *P*-value < 0.05.

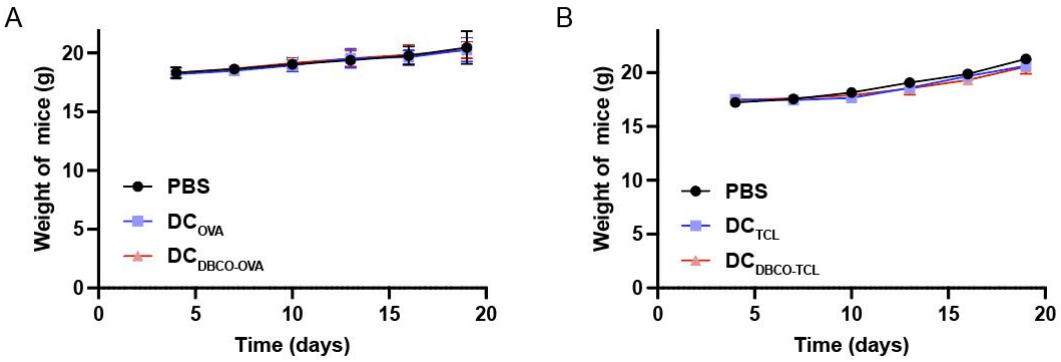

Figure S8. Body weight changes in mice after DC adoptive transfer. (A) Body weight monitoring of B16-OVA-bearing mice receiving adoptive transfer of DCs treated with DBCO-OVA or OVA alone. (B) Body weight monitoring of B16-F10-bearing mice receiving adoptive transfer of DCs treated with DBCO-TCL or TCL.

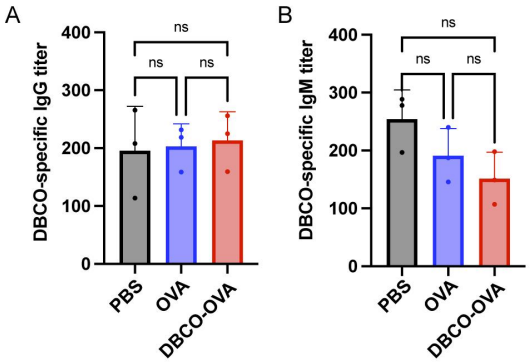

Figure S9. DBCO-OVA does not induce off-target immunity against the chemical linker. The titer of DBCO-specific IgG (A) and IgM (B) in mouse serum (n = 3 mice/group). Statistical analysis was performed using one-way ANOVA, and data are presented as mean ± SD. ns, no significance.

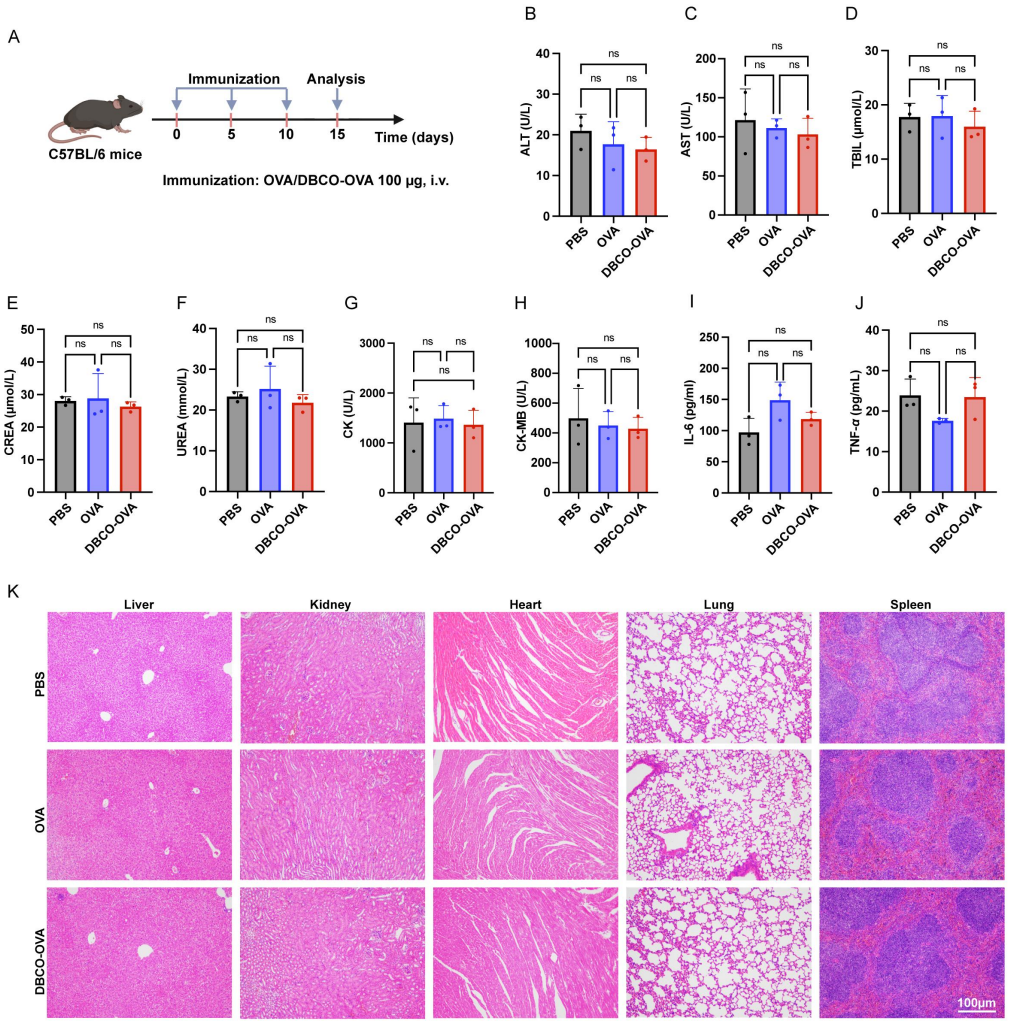

383

384 **Figure S10. Biosafety evaluation of DBCO-OVA treatment in C57BL/6 mice.** (A)
385 Schematic of the DBCO-OVA treatment protocol. C57BL/6 mice received i.v. OVA or
386 DBCO-OVA (100 μg) as indicated on day 0, 5, 10. On day 15, sera were collected for
387 biochemical analysis. Liver, kidney, heart, lung and spleen were collected for H&E
388 staining. (B-H) Quantification of serum ALT (B), AST (C), TBIL (D), CREA (E), UREA (F),
389 CK (G), CK-MB (H). (I and J) Quantification of serum IL-6 (I) and TNF-*α* (J). (K) H&E
390 staining in liver, kidney, heart, lung and spleen were shown, scale bar, 100 *μ*m. n = 3
391 mice/group. In K, the representative images from three independent mice were shown.
392 Statistical analysis was performed using one-way ANOVA, and data are presented as
393 mean ± SD. ns, no significance. Panel A created with BioRender.com.

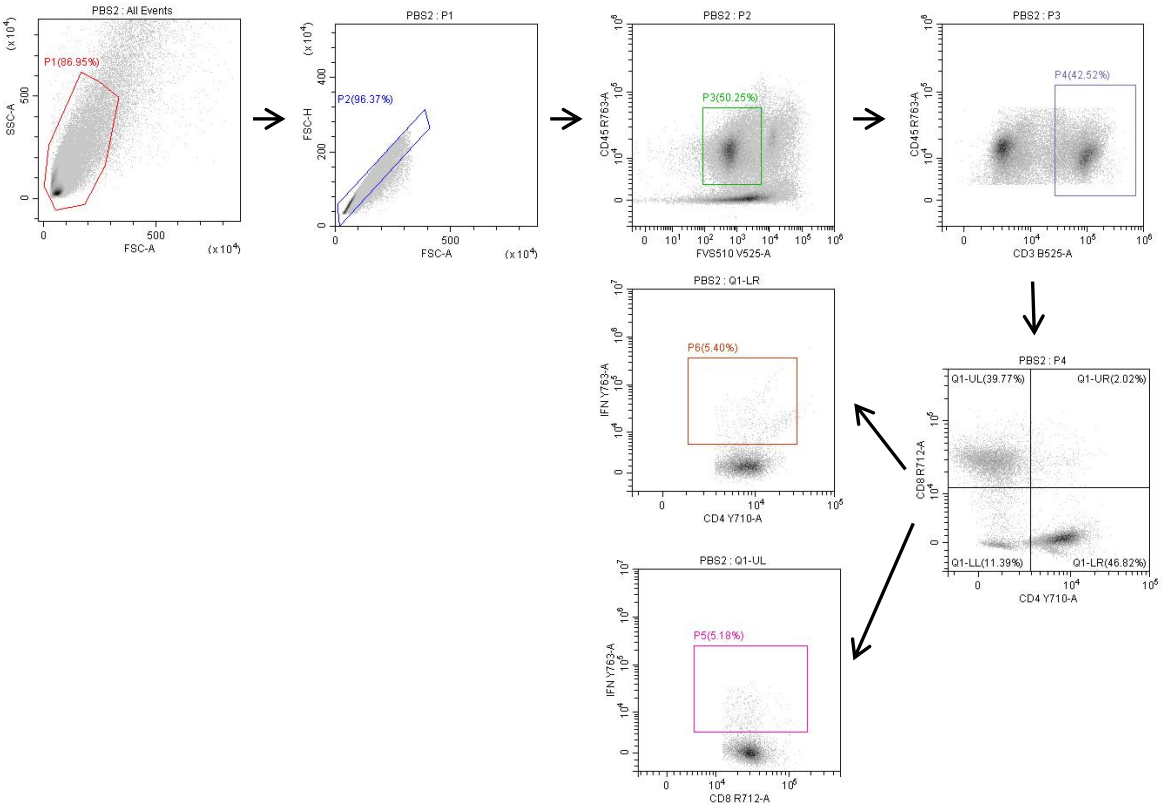

394

395 **Figure S11. Gating strategy for IFN-γ⁺ T cells in tumor tissues.**

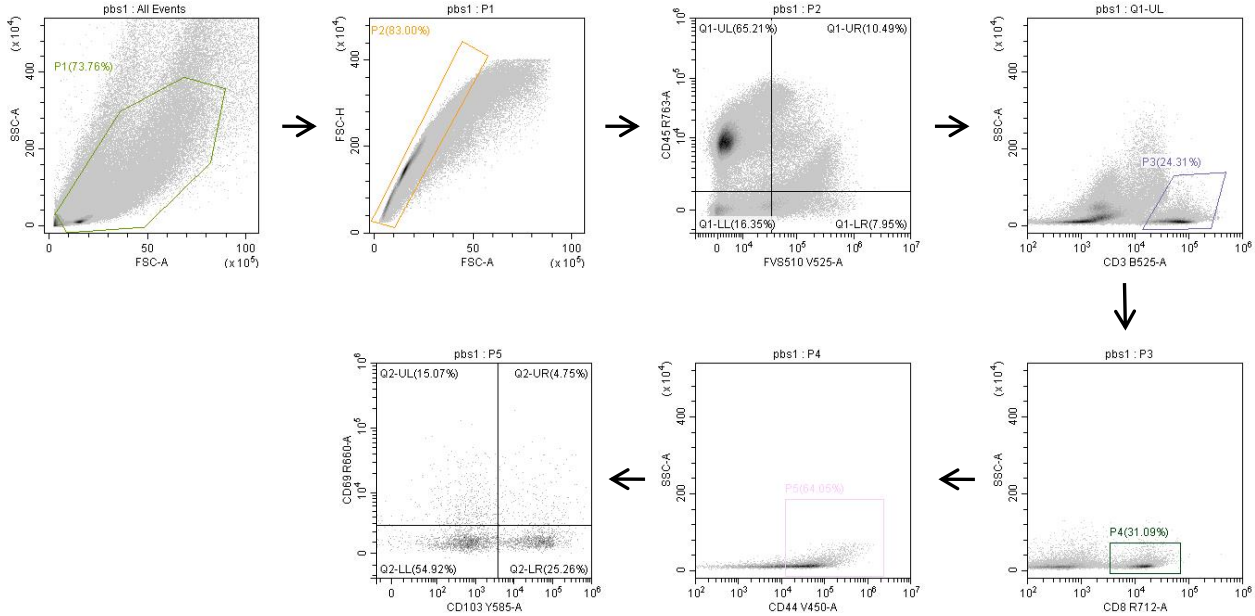

Figure S12. Gating strategy for tissue-resident memory T cells in tumor tissues.

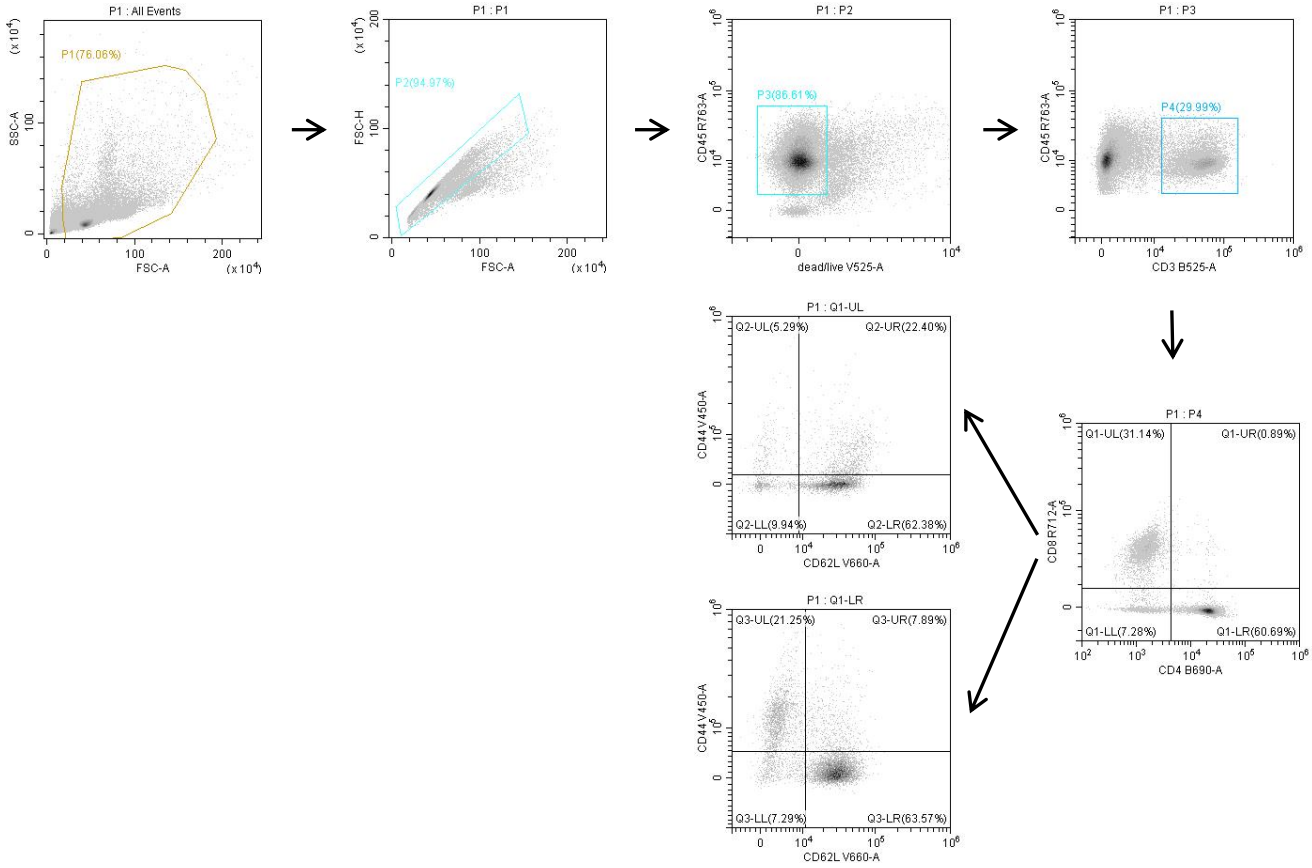

398

399 **Figure S13. Gating strategy for memory T cells in spleen.**

Table S2. Detection of ANA concentration in mouse serum from different treatment groups by chemiluminescence.

Group	ANA			
	Method	Results	Units	Reference Range
PBS	CL	< 2.00	RU/mL	< 20.00
OVA	CL	< 2.00	RU/mL	< 20.00
DBCO-OVA	CL	< 2.00	RU/mL	< 20.00

note: n = 3 mice/group

Table S3. Detection of Anti-Sm antibodies in serum from differently treated mice by immunofluorescence assay.

Group	anti-Sm antibody		
	Method	Results	Reference Range
PBS	IFA	< 1:80	< 1:80
OVA	IFA	< 1:80	< 1:80
DBCO-OVA	IFA	< 1:80	< 1:80

note: n = 3 mice/group

REFERENCES

(1) Denton, A. E.; Wesselingh, R.; Gras, S.; Guillonneau, C.; Olson, M. R.; Mintern, J. D.; Zeng, W.; Jackson, D. C.; Rossjohn, J.; Hodgkin, P. D.; Doherty, P. C.; Turner, S. J. Affinity Thresholds for Naive CD8+ CTL Activation by Peptides and Engineered Influenza A Viruses. J Immunol 2011, 187 (11), 5733–5744.

(2) Eberhardt, J.; Santos–Martins, D.; Tillack, A. F.; Forli, S. AutoDock Vina 1.2.0: New Docking Methods, Expanded Force Field, and Python Bindings. J Chem Inf Model 2021, 61 (8), 3891–3898.

(3) Trott, O.; Olson, A. J. AutoDock Vina: Improving the Speed and Accuracy of Docking with a New Scoring Function, Efficient Optimization, and Multithreading. J Comput Chem 2010, 31 (2), 455–461.